Cadmium impairs heart ventricular formation and disrupts polysialylated-NCAM/FGF receptor signaling in Xenopus tadpoles

Pélagie Douchez, Ingrid Fliniaux, Yoshiko Takeda-Uchimura, Alain Martoriati, Matthieu Marin, Anne Harduin-Lepers, Katia Cailliau

Cell & Bioscience

https://doi.org/10.1186/s13578-026-01579-y

Article in Press

Cadmium impairs heart ventricular formation and disrupts polysialylated-NCAM/FGF receptor signaling in *Xenopus* tadpoles

Received: 9 January 2026

Accepted: 19 April 2026

Published online: 03 May 2026

Cite this article as: Douchez P., Fliniaux I., Takeda-Uchimura Y. *et al.* Cadmium impairs heart ventricular formation and disrupts polysialylated-NCAM/FGF receptor signaling in *Xenopus* tadpoles. *Cell Biosci* (2026). https://doi.org/10.1186/s13578-026-01579-y

Pélagie Douchez, Ingrid Fliniaux, Yoshiko Takeda-Uchimura, Alain Martoriati, Matthieu Marin, Anne Harduin-Lepers & Katia Cailliau

Cadmium Impairs Heart Ventricular Formation and Disrupts Polysialylated-NCAM/FGF Receptor Signaling in *Xenopus* Tadpoles

Pélagie Douchez, Ingrid Fliniaux, Yoshiko Takeda-Uchimura, Alain Martoriati, Matthieu Marin, Anne Harduin-Lepers, Katia Cailliau*

Univ. Lille, CNRS, UMR 8576-UGSF-Unité de Glycobiologie Structurale et Fonctionnelle, F-59000 Lille, France

***** Corresponding author: Katia Cailliau Maggio. Email: katia.maggio@univ-lille.fr

Abstract

Background. Exposure to cadmium, a trace metallic element, is a major health concern. Cadmium is associated with a higher risk and predisposition to cardiovascular disease. Identifying molecular targets involved in such an effect is complexified by *in utero* embryonic and fetal development.

Methods. To overcome those difficulties, we used the established vertebrate heart model of *Xenopus laevis* to analyze the neural cell adhesion molecules NCAM and FGF receptors involved in early cardiac development under cadmium treatment. Cadmium exposure is performed from fertilization until the completion of mature heart development at the end of stage 45. Additional molecular modifications occurring within the heart are detected in the expressing signaling system of *Xenopus* oocytes.

Results. Exposure to cadmium results in the absence of heart ventricular myocardial trabeculae and disrupts the regulation of NCAM adhesion molecules and FGF receptor signaling in *Xenopus*. An increase in polysialylation (PSA) of NCAM is observed, accompanied by the deregulation in the expression of Golgi effectors Rab11 GTPase and Golph3. The sialyltransferases *ST8Sia2* and *ST8Sia4* are not increased at the transcriptional level but are accumulated in the Golgi apparatus. The highly sialylated NCAM interacts with the FGF receptor, prevents the formation of a complex with Integrin, FAK is *O*-GlcNAcylated, and the receptor translocation to the nucleus is impaired. Furthermore, the polysialylated-NCAM/FGF receptor signaling recruits higher amounts of Shp2 and leads to Erk2 hyperphosphorylation. Additionally, blocking FAK with a specific antibody in the normal polysialylated-NCAM/FGF receptor signaling causes the deregulated molecular phenotype.

Conclusions. These results represent a significant advancement for future studies in environmental toxicology and cardiac developmental dysfunctions resulting from cadmium exposure.

Highlights

Cadmium exposure led to the loss of ventricular myocardial trabeculae and the disruption of polysialylated NCAM/FGF receptor signaling.

Polysialylation of NCAM is increased and related to an accumulation of Golgi ST8Sia2 and ST8Sia4 sialyltransferases and a deregulation of Rab11 and Golph3 effectors in the Golgi.

FGF receptors complex formation with integrin is blocked, FAK is *O*-GlcNAcylated, Shp2 is highly recruited, and FGFR1 nuclear translocation is prevented.

Keywords

Cadmium, Heart, *Xenopus,* Polysialic acid, NCAM, FGF receptors, FAK, *O*-GlcNAcylation, Golgi apparatus.

Introduction

Cell adhesion molecules are essential for normal cardiac function, establishing specialized cell to cell contacts, and are postulated to be necessary for normal electrical coupling and mechanical contraction. Among them, the neural cell adhesion molecules (NCAM) are important components of the vertebrate developing nervous system and are also found in other developing and adult tissues [1–5]. NCAM are expressed in the fetal human heart [6], in the three layers of the developing heart epicardium, myocardium, and endocardium, in avian [7–9], in rat [10], and in *Xenopus* embryos [3]. In mouse, NCAM are also present in the embryonic developing heart and required for the ventricular conduction system development [11]. Evidence demonstrates that an NCAM increase is associated with heart failure and adverse left ventricular remodeling [12].

NCAM are cell membrane-associated glycoprotein members belonging to the family of immunoglobulin (Ig)-like proteins. They have five repeated Ig-like domains exposed on the extracellular surface, which serve as homophilic and heterophilic ligands [13]. The heterophilic heparin-binding site and the homophilic NCAM-binding site are attached to the second and third Ig-like domains, and the modulating post-translational modification of polysialic acid (PSA) moieties is set within the fifth domain. The negatively charged and highly hydrated PSA on NCAM is synthesized by two poly-α2,8-sialylatransferases [14,15] and occupies a large volume reducing adhesion and cell-to-cell interactions [1]. PSA defects on NCAM are associated with various pathologies mainly in the nervous system [15,16]. However, PSA-NCAM can also regulate other developing organs [17]. In the heart as in the neural system [18,19], PSA-NCAM play a dominant role in the differentiation of Purkinje cells and within the ventricular conduction system [11]. Evidence has demonstrated that pathologies affecting the network of developing Purkinje cells also increase the risk of cardiac death [20].

NCAM perform homophilic and heterophilic interactions. Stimulation of NCAM and NCAM interaction with FGF receptors (FGFR) initiate signaling pathways [21,22]. NCAM modulate FGFR that participates in the development of many organs, including the mesoderm-derived heart [23]. The FN3 domains of NCAM mediate interaction with the Ig2–3 regions of FGFR1 and FGFR3, initiating signaling cascades through inhibition of FGFR ubiquitination and degradation [24]. NCAM also affect FGFR cellular trafficking and promote stabilization of FGFR1 by recycling it to the cell surface through Rab11 GTPase and Src cytoplasmic kinase [25].

Cadmium, a metallic trace element released by human activities, has strong teratogenic and mutagenic effects. Low amounts of cadmium can negatively impact cardiovascular health (e.g. myocardial infarction [26], stroke, and heart failure [27,28]), although the precise molecular effects are unclear and few treatments exist [29,30]. Early cadmium exposure effects on the cardiovascular

system of embryos and fetuses are difficult to study in mammals and require models. The amphibian *Xenopus laevis* can be used to investigate the impact of pollutants, including metallic trace elements [31,32]. The choice to use the *Xenopus* embryo to study the early stages of heart development is supported by factors beyond its applicability in ecotoxicology. *Xenopus* has long been used to investigate heart development [33,34] and serves as a model to study congenital heart diseases [35]. During early development, a period proceeds without functional circulation, allowing for a comprehensive assessment of alterations in cardiovascular development [36]. Moreover, individual embryos, instead of mammalian *in vitro* cardiomyocyte cultures, allow direct assessment of three-dimensional structural and organizational changes during the formation of ventricular trabeculae, which cannot be achieved with cardiomyocyte culture models. We formerly published biometric parameters analysis of cadmium-treated stage 45 *Xenopus*, at a concentration that could be found in polluted spots, and the highest concentration allowing survival. We determined that exposure to 15 µM $CdCl_2$ resulted in a significantly lower length and a smaller eye gap compared to unexposed controls. The smaller body size of treated tadpoles was accompanied by a significant beat increase of the mature heart [37].

To identify and characterize the additional effect of cadmium exposure in the early developmental process of heart formation, we conducted exposure from fertilization and throughout the period of heart development and performed histological and biochemical examinations of the *Xenopus* heart. We found abnormal heart development and a significant increase in the quantity of PSA associated with NCAM. This increase was not attributable to an elevated expression of the sialyltransferases ST8Sia2 or ST8Sia4 but rather correlated with an enhanced presence of these enzymes in the Golgi apparatus and in changes in the levels of trafficking regulators Golgi phosphoprotein 3 (Golph3) and the small GTPase Rab11. The elevated levels of PSA on NCAM led to dysfunctional Fibroblast Growth Factor Receptor (FGFR) signaling. The recruitment of Integrin and Focal Adhesion Kinase (FAK) was decreased, and FAK was *O*-GlcNAcylated. These modifications were associated with an increase in Shp2 docking by the receptor complex and enhanced Erk2 phosphorylation, along with a lack of FGFR nuclear shuttling. In the *Xenopus* oocyte model, a signaling expressing system, we proved FAK immunoblockade shifted PSA-NCAM/FGFR signaling to a cadmium abnormal phenotype. Development under cadmium exposure generates molecular signaling abnormalities and should be considered as a cardiac threat in this context.

Results

Cadmium modifies heart ultrastructure, PSA on NCAM, and signaling effectors

Cadmium exposure was undertaken from fertilization to stage 45, until the mature heart is formed (Fig. 1A), at a concentration of 15 µM previously determined as a concentration found in the polluted environment at a highest and a limit for survival [37]. At stage 45, cadmium exposure results in abnormal heart characteristics compared to controls. The phenotype observed was an underdeveloped ventricle composed of a thick inner layer (where the cardiomyocytes are located), and lacking the typical trabeculae found at this stage. *Xenopus* showed an outflow tract and an inside spiral septum correctly shaped; the atria and the septum separating the left and right were visible; the atrioventricular valve was present (Fig. 2A). The number of trabeculae was significantly reduced with a mean of 1.5 ± 1.604 compared to untreated controls 5.714 ± 0.756 ($p = 1.094.\ 10^{-3} < 0.01$) (Fig. 2B).

Cadmium induces a significant increase in PSA in hearts at stage 45, as shown in western blots ($p = 5.732 \times 10^{-5} < 0.001$) (Fig. 3A). The specificity of the antibody toward PSA was confirmed by digestion of PSA (sialic acid chain of over seven residues) by endoneuraminidase. Immunoprecipitations of heart NCAM clarified that the amount of PSA carried by heart's NCAM 180 kDa is significantly increased ($p = 7.495 \times 10^{-3} < 0.01$) (Fig. 3B). NCAM 180 kDa is the only form detected. Negative controls using IgG ascertain the immunoprecipitation specificity. NCAM is among a limited number of glycoproteins that possess PSA. Following immunoprecipitation of NCAM, no detectable PSA remained in the residual extract (Fig. 3B).

To decipher the mechanism involved in PSA increase on NCAM after cadmium treatment, RT-qPCRs were performed to assess the levels of sialyltransferases *ST8Sia2* and *ST8Sia4* transcripts, which participate in PSA synthesis, and of *Neu1,* which codes for a sialidase that catalyzes the removal of sialic acid moieties from glycoproteins. The average copy number of *NCAM, Neu1, ST8Sia2*, and *ST8Sia4* per ten thousand copies of *histone H4* were not significantly different ($p > 0.05$, Student's t-test) (Fig. 4A). The calculated expression ratio for each transcript in cadmium-treated *versus* control conditions within each fertilization revealed no significant difference (Fig. 4B).

Analysis of molecular effectors in heart by western blots revealed that NCAM, FGFR1, Src, Shp2, Integrin, and FAK were present in the same quantities after cadmium treatment compared to controls (Fig. 5A). Golgi apparatus effector Golph3 was significantly increased ($p = 3.213.\ 10^{-3} < 0.01$, Student's t-test), while Rab11 GTPase was present in a significantly lower amount under cadmium conditions ($p = 3.547 \times 10^{-5} < 0.001$) (Fig. 5A). Erk2 displayed a higher level of phosphorylation in cadmium-treated heart ($p = 8.049 \times 10^{-5} < 0.001$) (Fig. 5B).

Immunoprecipitation of heart FGFR1 further reveals that FGFR1 forms a complex anchoring PSA, Src, Shp2, Integrin, and FAK in controls (Fig. 5C), ascertained by reverse immunoprecipitation of Integrin (Fig. 5D). IgG control immunoprecipitations confirm the specificity of the anchored effectors.

After cadmium exposure, immunoprecipitation of FGFR1 showed that its phosphorylation occurs to the same extent compared to controls. To the contrary, FGFR1 is co-precipitated with Integrin and FAK to a significant lower extent (Fig. 5C), and Src is not recruited by FGFR1 (Fig. 5C) and not found in the Integrin immunoprecipitates after cadmium treatment (Fig. 5D). Significant differences are in Fig. 5C for Src ($p = 2.897 \times 10^{-2} < 0.05$), Shp2 ($p = 9.275 \times 10^{-4} < 0.001$), Integrin ($p = 3.253 \times 10^{-4} < 0.001$), FAK ($p = 8.144 \times 10^{-7} < 0.001$), and in Fig. 5D for FGFR1 ($p = 5.674 \times 10^{-13} < 0.001$), and FAK ($p = 5.718 \times 10^{-13} < 0.001$).

Moreover, FAK is *O*-GlcNAcylated in FAK immunoprecipitates with a significant difference ($p = 3.369 \times 10^{-5} < 0.001$) (Fig. 5E) under cadmium conditions. FAK *O*-GlcNAcylation is confirmed by a WGA pulldown (Fig. 5F) and a GlcNAc control for the specificity (Fig. 5F).

Further experiments using Golgi apparatus purification allowed the detection of higher quantities of ST8Sia2 and ST8Sia4 in cadmium-exposed hearts compared to controls ($p = 1.65 \times 10^{-4} < 0.001$ and $p = 3.028 \times 10^{-2} < 0.05$, respectively) (Fig. 5G). GM130 and TGN46 markers, respectively, ascertain Golgi and vesicle fractions (Fig. 5G).

PSA-NCAM/FGFR signaling is highly rewired

To gain better insight into the consequences of PSA increase on NCAM and the potential signaling modifications, FGFR1 was expressed in the *Xenopus* oocyte system (Fig.1B), followed by the detection of signaling effectors recruitment. NCAM isolated from control hearts (NCAM) and from cadmium-treated hearts (NCAMCd) were immunoprecipitated and eluted before they were used to stimulate FGFR1-expressing oocytes and compared to FGF2 ligand stimulation. The higher quantity of PSA on NCAMCd eluted from the immunoprecipitates was confirmed ($p = 5.119 \times 10^{-5} < 0.001$, Student's t-test, upper histogram) (Fig.6A). Before its use to stimulate FGFR1-expressing oocytes, the quantity of eluted PSA on NCAM and eluted PSA on NCAMCd was confirmed to be equivalent to the immunoprecipitated and directly blotted PSA from NCAM and NCAMCd in Figure 3B ($p = 9.067 \times 10^{-2}$, lower histogram) (Fig. 6A). In the oocyte expressing system, FGF2, NCAM, and NCAMCd stimulations confirmed results obtained directly on the control and cadmium-treated hearts (Fig. 6B). FGFR1 recruits the Grb2 adaptor under eluted control NCAM, eluted NCAMCd, or FGF2 stimulations. Only control NCAM stimulation allowed FGFR1 to recruit Src. NCAMCd allowed a higher level of Shp2 binding compared to control NCAM in the FGFR1 immunoprecipitates, with none under FGF2 stimulation. NCAMCd also recruited less Integrin and FAK than the control, with no recruitment observed in the presence of FGF2. Figure 6B shows significant differences with lower amounts for Src ($p = 1.072 \times 10^{-5}$), Integrin ($p = 5.854 \times 10^{-7} < 0.001$), FAK ($p = 2.63 \times 10^{-5} < 0.001$), and a higher amount for Shp2 ($p = 1.243 \times 10^{-8} < 0.001$). Results were ascertained by reverse Integrin immunoprecipitations (Fig. 6C) showing significantly lower amounts of FAK ($p < 7.46 \times 10^{-16}$) and Src ($p < 2.2 \times 10^{-16}$).

FAK was *O*-GlcNAcylated only in the NCAMCd condition ($p = 3.34 \times 10^{-6} < 0.001$) (Fig. 6D) and associated with a higher Erk2 phosphorylation compared to control conditions ($p = 1.655 \times 10^{-4} < 0.001$) (Fig. 6E).

Microinjection of FAK antibodies to inhibit FAK recruitment by FGFR1 led to abnormal effector recruitments by FGFR1, resembling the effects observed following cadmium exposure. FAK, Integrin, and Src were not present in complex with FGFR1. Shp2 was present in high quantity (Fig. 6F). FAK was *O*-GlcNAcylated (Fig. 6G), and Erk2 was hyperphosphorylated (Fig. 6H).

Further analyses were undertaken to localize FGFR1 intracellularly and decipher potential nuclear translocation. Enucleation of oocytes allowed direct separation of the nucleus from the cytoplasm and the membrane fractions. With FGF2 stimulation, FGFR1 was primarily found in the membrane and nucleus; under control conditions, FGFR1 was evenly distributed among the membrane, cytoplasm, and nuclear fractions (Fig. 6H). NCAMCd stimulation allowed more FGFR1 to be localized into the cytoplasm compared to the amount present in the membrane, and no FGFR1 was detected in the nucleus (Student's t-test, $p = 2.2 \times 10^{-16} < 0.001$). With NCAM stimulation and FAK antibody treatment, FGFR1 was absent from the nucleus ($p = 1.049 \times 10^{-10} < 0.001$), increased in the membrane, and remained unchanged in the cytosol. With NCAMCd stimulation and FAK antibody, FGFR1 was found in the membrane and cytosol, but not in the nucleus, similarly to NCAMCd stimulation without FAK antibodies. With FGF2 stimulation and FAK antibody, FGFR1 localized into the nucleus and membrane, and was more abundant in the cytosol than with FGF2 stimulation alone. Actin, Erk2, and Histone H3 served as internal controls, respectively for membrane, cytoplasm, and nuclear fractions (Fig. 6H).

Heart control features (Fig.7A) were changed under cadmium exposure (Fig.7B), resulting in no ventricular myocardial trabeculae, altered Golgi apparatus enzymes, and disrupted PSA-NCAM/FGFR signaling. Normally, the Golgi apparatus was shown to contain Rab11, Golph3, and polysialyltransferases. Additionally, PSA-NCAM was complexed with FGF receptor and Integrin, recruiting FAK, low Shp2, and allowing Erk2 phosphorylation and nuclear translocation of FGFR. Cadmium deregulation increased PSA on NCAM, and favored a decrease of Rab11, a rise in Golph3, and an accumulation of ST8Sia2 and ST8Sia4 in the Golgi apparatus. The excess of PSA on NCAM consequently rewired FGFR signaling, bypassing Integrin/FAK and modifying FAK with an *O*-GlcNAcylation.

Discussion

Cadmium lowers trabeculation in the heart and increases PSA on NCAM *via* Golgi deregulation

The *Xenopus* heart encompasses two atria separated by a septum, a single trabeculated ventricle, and an outflow tract. We have shown that cadmium critically impacts trabeculae formation during heart development. The heart chamber appeared composed of normal OFT and atria, but the ventricle lacked the characteristic trabeculae normally present in its inner wall. These trabeculations appear to play an essential role in cardiac embryology. Due to an increased contact surface with circulating blood, they allow a supply of oxygen and nutrients to the myocardial muscle [38]. The ventricular trabeculae that develop as a network of cardiomyocytes are critical for the conduction system and the ventricular chamber maturation, processes highly conserved across vertebrate evolution [39, 40]. However, factors controlling the development and patterning of the trabeculae are still under investigation and seem to require the regulation of cell adhesion, polarity, cytoskeleton, and tension effectors.

Cellular adhesion effector NCAM play an important role in vertebrate heart throughout development where they have been detected (avian [41], rat [42], mouse [43], and human [44] in association with myocardial [45], endocardial (avian [8,9,10]), epicardial cells (rat [10]), and heart nerves [10,45]. The 180 kDa NCAM is the primary form found in the *Xenopus* embryonic/tadpole heart at stage 45, with no other forms detected in our study or reported in the literature [3,37,46,47]. PSA-NCAM was strongly detected in the myocardial trabeculae in close connection with the atrioventricular canal [48]. Abnormal cardiac signaling could impact this process. In our experiments, the heart NCAM transcript and protein levels did not change after cadmium exposure compared to untreated controls. Additionally, NCAM are shown to carry more post-translational polysialylation under cadmium exposure. Regulation of NCAM polysialylation is crucial not only in neural development, where it was abundantly studied, but also in cardiac development [11,49]. PSA changes are associated with several cardiac diseases [50]. Sialyltransferases ST8Sia2 and ST8Sia4 are the two known enzymes responsible for polysialylation in vertebrates [15,51,52]. At the transcriptional level, no significant differences were found that could account for the higher level of PSA on NCAM under cadmium exposure. However, the detection of these enzymes revealed that their number is more important in the Golgi fraction after cadmium treatment. Two modulators associated with Golgi enzymes and vesicular transport were also deregulated. A decrease in Rab11 due to cadmium exposure could ensure that more polysialyltransferases are localized in the Golgi and enhance polysialylation on heart NCAM. Rab11 GTPase has been shown to be a key player in Golgi transport and endosomes recycling, and it is involved in the negative regulation of sialylation by affecting sialyltransferases transport [53,54]. The knockdown of Rab11 impairs endosomal transport, results in an accumulation of sialyltransferases inside the Golgi, and finally enhances the degree of sialylation [53]. Golph3, another essential effector necessary for efficient Golgi trafficking [55], is increased in the presence of cadmium and may facilitate the transport of PSA-NCAM. Golph3 was shown to anchor sialyltransferases from the ST6Gal family

and to regulate sialylation on cell surface proteins without regulating gene expression levels of sialyltransferases. It is known that Golph3 depletion generates altered subcellular localization of Golgi sialyltransferase enzymes and lower sialylation [56]. We can hypothesize that under cadmium conditions in the heart, a decrease in Rab11 in the Golgi apparatus would impair endosomal transport, leading to an accumulation of polysialyltransferases and an increase in PSA-NCAM. Additionally, the rise in Golph3 level would enhance trafficking to the plasma membrane, contributing to an increase in PSA-NCAM. The efficiency of Golgi enzymes in processing their substrates and the amount of glycans produced are influenced by the composition of the Golgi lumen [57,58]. The exocytic and endocytic compartments of the Golgi apparatus have distinct luminal ion compositions, which include calcium (Ca^{2+}) and manganese (Mn^{2+}) [57,59]. Failure to maintain this ion homeostasis negatively impacts glycosylation, membrane trafficking, and protein sorting [57,59]. Cadmium (Cd^{2+}) ions may substitute for other essential divalent ions [59,60,61], potentially by replacing Ca^{2+} and/or Mn^{2+} in the TMEM165 Golgi antiport and reducing their availability in the Golgi lumen [62,63,64]. Such alteration would affect the activity of sialyltransferases and galactosyltransferases in the Golgi [14], the recycling of endosomes [54], molecular signaling effectors [58,65], and membrane receptors [66], with a subsequent reduction of Rab11 and an increase in Golph3 levels.

PSA increase on NCAM deregulates FGFR signaling

The consequences of PSA increase on NCAM were further analyzed with respect to FGFR signaling, which is required for heart development in vertebrates [67] (in *Xenopus* [68], zebrafish [69], mouse [23,70], and human [71]). FGFR1 is essential for cardiomyocyte development [72]. FGFR signaling deregulation is linked to several heart syndromes and diseases [23,73–75], and to inflammatory cardiopathy [76]. Furthermore, mutations of the FGF/FGFR signaling in mice lead to congenital heart defects [77]. Additionally, FGFR1 is also involved in Golgi organization and function [78].

Elution of immunoprecipitated PSA-NCAM allowed the recovery of a PSA with a length ranging from 250 to 150 kDa, similar to the PSA extracted from isolated hearts in our experiments. Reconstitution of PSA-NCAM 180 kDa/FGFR signaling allowed similar recruitment and deregulation of effectors under cadmium exposure. Our results agree with former signaling studies describing different dynamics for FGFR1 receptor recruitment under FGF2 or NCAM activation [79]. NCAM is described to induce the formation of FGFR1 complexes and to trigger Erk2 phosphorylation in a Src-dependent manner, whereas FGF binding is independent of Src [79]. In our experiments, the deregulation by cadmium increases the amount of PSA and promotes signaling without Src and with Erk2 higher phosphorylation. Cadmium also results in reduced recruitment of Integrin and FAK to FGFR1, coinciding with the *O*-GlcNAcylation of FAK, two key signaling events. FAK is an important

signaling integrator that alters cardiac growth and homeostasis, attenuates cardiac fibrosis, and post-myocardial infarction [80]. FAK sets downstream Integrin and upstream Src and Erk2 [81] and is associated with FGF and NCAM signaling [82]. Moreover, *O*-GlcNAcylation regulates Integrin- and FAK-mediated cell adhesion [83]. Recent findings indicate that a low level of *O*-GlcNAcylation on FAK at specific sites, including Ser708, Thr739, and Ser886, are associated with increased binding affinity to integrins and enhanced migration capabilities [84]. This observation supports our findings regarding the disrupted interaction between highly *O*-GlcNAcylated FAK and integrins under cadmium conditions, and the fact that migration of myocardial cells, which typically occurs during normal cardiogenesis to form heart trabeculae [85], is inhibited in cadmium conditions. By experimental downregulation of FAK, the NCAM normal signaling phenotype shifted to a cadmium-type phenotype, encompassing Shp2 deregulation and high Erk2 phosphorylation [86]. Our former work described that tadpoles submitted to cadmium are significantly smaller with higher beat counts in the just-formed mature heart [37]. Interestingly, despite the significant anatomical and physiological differences between amphibians and mammals, some conserved signaling pathways appear to be shared. Xenopus has a three-chambered heart, consisting of two atria and a single ventricle, while mammals have a four-chambered heart. However, both groups exhibit commonalities at the molecular level, particularly with the hyperactivation of Shp2 and Erk. This molecular pattern of hyperactivation is detected in the Noonan syndrome, where the second most common cause of this congenital heart disease is associated with cardiomyopathy and ventricular defects [87-90]. Finally, cadmium inhibits FGFR1 nuclear addressing and could modify specific transcriptional control [91,92].

Conclusions

Our findings identify that specific molecular changes associated with cadmium disruption of heart development are summarized in Fig.7. Specifically, ventricular trabeculae and PSA on NCAM are deregulated in addition to Golgi abnormalities and lead to dysfunctional interactions between PSA-NCAM and FGF receptors. Molecular targets, such as FAK and the polysialylation machinery, could be used for the detection of cadmium-induced heart defects.

Materials and methods

Ethical statement, and animal handling

All procedures are conformed to the guidelines from Directive 2010/63/EU of the European Parliament on the protection of animals used for scientific purposes and the use of Laboratory Animals.

The protocols were approved by the University of Lille institutional board (Comité d'Ethique en Expérimentation Animale, Haut de France, G59-00913).

Xenopus laevis were purchased from TEFOR (Paris, Saclay, France) and were housed in PHExMAR at the University of Lille. To collect gonads for oocytes and sperm, *Xenopus* were euthanized by total immersion in 5 g/L MS222 (3-Aminobenzoic acid ethyl ester Methanesulfonate) for 1 hour. Subsequent decerebration and demedullation were performed on the brainstem of adult *Xenopus*. Spawning was induced by the injection of one dose of human chorionic gonadotropin (700 U) in the female's dorsal lymph sacs (final volume 200 µL). Twenty-four hours later, gentle pressure was applied to the animal's ventral side to obtain unfertilized eggs. Eggs were fertilized by the addition of small pieces of testis and a gentle mix, until the typical cortical rotation occurred, attesting to the success of fertilization. Fertilized eggs were dejellied for 10 minutes with 2 % L-cysteine with or without $CdCl_2$ 15 µM (2.5 mg/L) and rinsed three times. *Xenopus* embryos and tadpoles were kept in daily renewed sterilized water (pH 7.42), added or not with $CdCl_2$ at 19 °C. Stage 45 *Xenopus* (after 6 days of exposure with a formed and beating mature heart [93]) were chosen according to the Nieuwkoop and Faber table [94]. Hearts were extracted under a binocular microscope and immediately collected in the tissues lysis buffer for RNA extraction or in western blot (WB) lysis buffer.

RNA preparation, microinjection into the expressing system, and treatments

FGFR1 inserted into pSP64T vector was used to generate capped cRNAs using SP6 RNA polymerase (mMESSAGE mMACHINE kit, Ambion) as previously described [95].

Ovarian lobes were stored at 14 °C in ND96 medium (96 mM NaCl, 2 mM KCl, 1.8 mM $CaCl_2$, 1 mM $MgCl_2$, 5 mM HEPES-NaOH, pH 7.5). Stage VI oocytes, used as an expressing system, were defolliculated by digestion with dispase (0.5 mg/mL) for 3 h and collagenase A for 45 min (0.5 mg/mL) in ND96 at 19 °C.

Sixty ng of FGFR1 mRNA were microinjected into stage VI oocyte expressing system in the equatorial region using a positive displacement digital micropipette (Nichiryo) and incubated at 19 °C in ND96 medium for 2 days. In some experiments, the microinjected oocytes were submitted to a second microinjection with anti-FAK antibodies 40 nL (2A7 Sigma–Aldrich). Expressing systems were incubated for 1 h in ND96, added or not with $CdCl_2$ 15 µM, before they were stimulated by FGF2 (5 nM), normal NCAM or cadmium-treated NCAMCd, and finally stored at 19 °C for 15 h with $CdCl_2$ 15 µM. During enucleation, oocytes were pinched at the animal pole, the nucleus was removed, and the cytoplasm and membrane fractions were collected.

Immunoprecipitations

Samples were lysed in the following PYT homogenization buffer: 50 mM HEPES (pH 7.4), 500 mM NaCl, 0.05 % (m/v) SDS, 0.5 % (v/v) Triton X-100, 5 mM $MgCl_2$, 1 mg/mL bovine serum albumin, 10 µg/mL leupeptin, 10 µg/mL aprotinin, 10 µg/mL soybean trypsin inhibitor, 10 µg/mL benzamidine, 1 mM PMSF, 1 mM sodium vanadate. 20 hearts or 10 oocytes expressing system were grouped. After a 12000 g centrifugation for 10 min at 4 °C, the supernatants were precleared for 1 h with protein A Sepharose (20 µL of 50 % beads/ 200 µL of lysate) at 4 °C under gentle rocking before incubation for 1 h with antibodies against Integrin β1 (M-106, Santa Cruz Biotechnology, 1/1500), FAK (2A7, Sigma–Aldrich; 1/1000 dilution), or FGF receptor (D8E4, Cell signaling technology, 1/1000) at 4 °C under rotation. An incubation of 1 h with protein A Sepharose (20 µL of 50% bead slurry) at 4 °C under rotation was afterwards realized. The bead pellets were rinsed 3 times in PYT buffer and resuspended in 4X Laëmmli buffer.

For NCAM immunoprecipitations, 20 hearts from stage 45 tadpoles were homogenized in RIPA buffer, at 4 °C (1 µL RIPA buffer/1 heart). After a 10 min centrifugation at 12000 g, supernatants were precleared with CNBr-Activated Sepharose™ 4B (GE Healthcare) for 1 h under rotation, at 4 °C. After a brief centrifugation, supernatants were incubated for 2 h at 4 °C with CNBr-Activated Sepharose™ 4B coupled to NCAM antibodies (100 µL extract/ 20 µL of 50% NCAM-CNBr beads). Coupling of NCAM antibodies to CNBr-Activated Sepharose™ 4B (GE Healthcare) was performed following the manufacturer's instructions. Extracts were rinsed 3 times with RIPA/PYT buffer (1V/1V). Elution was performed on centrifuged NCAM-CNBr beads with NaCl 1M (20 µL) immediately readjusted with 180 µL of ND buffer (2 mM KCl, 1.8 mM $CaCl_2$, 1 mM $MgCl_2$, 5 mM HEPES-NaOH, pH 7.5). Sample concentrations were measured and saved for activation experiments and partly resuspended in 4X Laëmmli buffer before SDS-PAGE and western blot (WB) were performed. 4 to 5 independent experiments were repeated.

Endoneuraminidase-N digestion

Samples prepared in PYT buffer were treated with 0.7 U of endoneuraminidase-N (Eurobio Scientific) at 37 °C for 1 h and resuspended in 4X Laëmmli sample buffer before western blot analysis.

Golgi isolation

The minute Golgi Apparatus Enrichment Kit (GO-037, Invent Biotechnologies) was used following the manufacturer's instructions. The procedure steps were performed at 4 °C unless specified. Briefly, 15 hearts were ground in buffer A (300 µL) and loaded onto a cartridge filter, before centrifugation for 30 s at 16000 g, followed by another 5 min at 5000 g. The supernatant was

transferred to a new tube and centrifuged for another 30 min at 16000 g. The supernatant was transferred to a new tube, while the pellet containing mitochondria, endoplasmic reticulum, lysosomes, and plasma membranes was discarded. Buffer B was added to the supernatant (ratio 1/1), placed for 10 min on ice, before centrifugation was performed for 5 min at 8000 g. The resulting supernatant SV containing secretory vesicles associated with trans-Golgi membranes was transferred to a new tube. The remaining pellet was resuspended in buffer A (150 µL) and centrifuged for 5 min at 8000 g. The supernatant was transferred to a new tube and added with buffer C (75 µL) and vortexed. After an incubation of 20 min on ice, centrifugation was performed to isolate the pellet containing the Golgi fraction for 10 min at 8000 g. For the vesicle fraction, buffer D (75 µL) was added to the supernatant SV, incubated for 20 min on ice, before centrifugation was performed for 5 min at 16000 g. The pellet contains the vesicle fraction. Finally, the fractions containing the Golgi apparatus or the secretory vesicles were separately resuspended in Laëmmli buffer.

Electrophoresis and western blot

Expressing oocytes and stage 45 hearts were lysed in homogenization buffer PYT with a ratio of 10 oocytes/100 µL of buffer or 20 stage 45 hearts in 20 µL of buffer. Protein concentrations were measured using the Bradford (BioRad) reaction and spectrophotometer (SPECTROstar Nano, BMG LABTECH).

For subcellular analysis, oocytes were manually enucleated (30 nuclei/10 µL in PYT buffer), their cytoplasm aspirated using a positive displacement digital micropipette (Nichiryo) (30 cytoplasm/150 µL PYT buffer), and the membrane and resuspended in PYT (30 membrane/50 µL PYT) before they were homogenized in a glass grinder at 4 °C.

After a 12000 g centrifugation for 10 min at 4 °C, the supernatants were denaturated in 2X Laëmmli buffer (65.8 mM Tris-HCl pH 6.8; 26.3 % (v/v) glycerol; 2.1 % (m/v) SDS; 0.01 % (m/v) bromophenol blue; 4% (v/v) β-mercaptoethanol, BioRad) for 3 min at 96 °C or at 60 °C for PSA analysis.

Protein concentration of supernatants was determined and adjusted if necessary, using BioRad assay at 595 nm (SPECTROstar Nano, BMG LABTECH) and adjusted if necessary.

Proteins were separated by 4-20% SDS-PAGE gels (mini protean TGX, BioRad) for 1 h at 200 V in denaturing buffer (0.1% (m/v) SDS; 0.3% (m/v) Tris base; 1.44% glycine). Transfers onto nitrocellulose membrane (Amersham Hybond) were performed by wet transfer (0.32% (m/v) Tris; 1.8% (m/v) glycine; 20% (v/v) methanol), at 100 V for 1 h.

Membranes were blocked with 5% (m/v) low-fat dry milk or bovine serum albumin added in TBS-Tween 0.05%. Incubation at 4 °C overnight with specific primary antibodies were realized using rabbit antibodies raised against histone H3 (9715, Cell signaling technology, 1/1000), Integrin (M-106, Santa Cruz Biotechnology, 1/1500), Shp2 (3752 Cell signaling technology, 1/1000), Src (2108 Cell

signaling technology, 1/1000), TGN46 (Sigma Aldrich, 1/1000); mouse antibodies raised against Erk2 (D-2 sc1647, Santa Cruz Biotechnology,1/1500), Tyr 202/204 phosphorylated Erk2 (Santa Cruz Biotechnology, 1/1000), FAK (2A7, Sigma–Aldrich; 1/1000 dilution), FGF receptor (D8E4, Cell signaling technology, 1/1000), Golph3 (Sigma-Aldrich, 1/1500), GM130 (Santa Cruz Biotechnology, 1/1000), phospho-tyrosine (PY20, Sigma-Aldrich, 1/1000), *O*-GlcNAc (RL-2, Thermo Fisher Scientific, 1/1200), Rab11 (Santa Cruz Biotechnology, 1/1500); and goat antibodies raised against Actin (Santa Cruz Biotechnology, 1/1200). After three washes of 10 min in TBS-Tween 0.05%, nitrocellulose membranes were incubated with the appropriate horseradish peroxidase-labelled secondary antibodies for 1 h: rabbit or mouse antibodies (Invitrogen, by Thermo Fisher Scientific Biosciences GMBH, 1/30000) or goat antibodies (Santa Cruz Biotechnology, 1/30000). After three washes in TBS-Tween 0.05%, signals were revealed with a chemiluminescent assay (ECL Select, GE Healthcare) on hyperfilms (Amersham MP). The membranes were stripped with the ready-to-use stripping buffer (Clinisciences). After confirming that the initial chemiluminescent signal was no longer present, the membranes were reprobed with the specified antibodies. Signals were quantified using Image J (Fiji Software, v1.52i) and normalized either using the respective Actin loading control, total Erk2 for the phosphorylated form of Erk2, or FAK for the *O*-GlcNAcylated form of FAK. For immunoprecipitation, normalization was based on the amount of each protein in the immunoprecipitation.

Succinylated Wheat Germ Agglutinin pull-down

Oocytes were lysed in PYT buffer as described. After a centrifugation at 12000g and 4 °C for 10 min, 200 µL lysates were incubated with 50 µL of succinylated-Wheat Germ Agglutinin (sWGA) agarose beads (Vector Laboratories) at 4 °C for 2 h or with 0.5 M free GlcNAc preincubated sWGA beads as a control. sWGA-bound proteins were washed three times and eluted in 4x Laëmmli buffer before SDS-PAGE.

cDNA synthesis and RT-qPCR

RNA was extracted from pools of 50 hearts of control or cadmium-treated stage 45 tadpoles from N = 6 different fertilizations using the RNeasy Plus® Micro Kit (Qiagen) according to the manufacturer's protocol. cDNA was synthesized starting from 500 ng of total RNA per sample, using 0.5 µg of random hexamers and 20 U of M-MLV reverse transcriptase (Promega). Reverse transcriptase-quantitative polymerase chain reaction (RT-qPCR) was performed from 1 µL of cDNA with Luna® Universal qPCR Master Mix (New England Biolabs) using SYBR® Green. Plasmids containing PCR products for each target were used as standards to perform absolute quantification, and the copy number of *H4 histone* cDNA was used for normalization. Primer sequences are: histone H4 (XM_041576342.1) 5'-GACGCTGTCACCTACACCGAG and 5'-CGCCGAAGCCGTAGAGAGTG, *ST8Sia2.L*

(NM_001087720) 5'-CTCGTCCACTTCAAGTACTGC and 5'-GGGTCCCCTTCAAAACCGAA, *ST8Sia2.S* (XM_018255305.2) 5'-TCGCTTCGCGCTCTCTCTTCC and 5'-TTGTGCCGCTCCCTCCAG, *ST8Sia4.L* (XM_018264470) 5'-CTTCGAAAGGAAGGTTCAGCG and 5'-AGACACGTCCCTTTCTGCGT, *ST8Sia4.S* (XM_018244337) 5'-CTTGGACGCAGAGAGGGATG and 5'-GCGACGGCTTTTCATAGGTG, *NCAM* matching both L. and S. genes (NM_001087829 and NM_001087827.1) 5'-CCTGGTGCCAAAGGCAAAGA and 5'-AGGTAGCATGTCCTCAACAGCA, *Neu1.L* (NM_001092613.1) 5'-TCGGAGTGCGCCCTATAAAC and 5'-ACGGAAAGTATCCACTTCACCA.

Heart histology

Samples were fixed in MEMFA, 1 mM $MgSO_4$, 2 mM EGTA, 3.7 % formaldehyde, 0.1 M MOPS at pH 7.4 for 2 h. They were rinsed, dehydrated, and embedded in paraffin. Sections of 7 microns were cut and stained with nuclear red (0.1% nuclear red in 5% aluminum sulfate) and picroindigo carmine (0.25% picroindigo carmine in saturated picric acid).

Statistics

Normality was assessed with the Shapiro-Wilk test to determine the appropriate statistical analysis. Student's t-test was used for normal distributions, while non-normal data were analyzed by the Wilcoxon Mann-Whitney test. For western blot analysis, the Student's t-test was used.

Ethics approval and consent to participate

All procedures are conformed to the guidelines from Directive 2010/63/EU of the European Parliament on the protection of animals used for scientific purposes and the use of Laboratory Animals. The protocols were approved by the University of Lille and the "Comité d'Ethique en Expérimentation Animale", Haut de France, G59-00913.

Consent for publication

All the listed authors have participated in the study and have seen and approved the submitted manuscript.

Availability of data and materials

The data underlying this article are available in the article.

Competing interests

The authors declare no competing interests.

Funding

This study was founded by the University of Lille and the CNRS.

Authors ' contributions

P.D, I.F., Y.U.K., A.M., M.M., and K.C. conceptualized, designed and performed experiments. P.D, I.F., Y.U.K., A.M., M.M., A.H.L., and K.C. wrote the manuscript and generated the figures. All authors commented, edited and approved the manuscript.

References

1. Yang P, Major D, Rutishauser U. Role of charge and hydration in effects of polysialic acid on molecular interactions on and between cell membranes. J Biol Chem. 1994;269:23039–23044.
2. Thiery JP, Duband JL, Rutishauser U, Edelman GM. Cell adhesion molecules in early chicken embryogenesis. Proc Natl Acad Sci U S A. 1982;79:6737–6741.
3. Sunshine J, Balak K, Rutishauser U, Jacobson M. Changes in neural cell adhesion molecule (NCAM) structure during vertebrate neural development. Proc Natl Acad Sci U S A. 1987;84:5986–5990.
4. Lackie PM, Zuber C, Roth J. Polysialic acid of the neural cell adhesion molecule (N-CAM) is widely expressed during organogenesis in mesodermal and endodermal derivatives. Differentiation. 1994;57:119–131.
5. Watanabe M. The Neural Cell Adhesion Molecule and Heart Development: What is NCAM Doing in the Heart? Basic Appl Myol. 1998;8:277–291.
6. Al-Mahdawi S, Shalial A, Wyse RKH. Neural cell adhesion molecule (N-CAM) in fetal and mature human heart. FEBS Lett. 1990;267:183–185.
7. Burroughs CL, Watanabe M, Morse DE. Distribution of the neural cell adhesion molecule (NCAM) during heart development. J Mol Cell Cardiol. 1991;23:1411–1422.
8. Crossin KL, Hoffman S. Expression of adhesion molecules during the formation and differentiation of the avian endocardial cushion tissue. Dev Biol. 1991;145:277–286.
9. Gerety M, Watanabe M. Polysialylated NCAM expression on endocardial cells of the chick primary atrial septum. Anat Rec. 1997;247:71–84.
10. Lackie PM, Zuber C, Roth J. Expression of polysialylated N-CAM during rat heart development. Differentiation. 1991;47:85–98.
11. Delgado C, Bu L, Zhang J, Liu FY, Sall J, Liang FX, Furley AJ, Fishman GI. Neural cell adhesion molecule is required for ventricular conduction system development. Dev. 2021; 148:dev199431

12. Nagao K, Sowa N, Inoue K, Tokunaga M, Fukuchi K, Uchiyama K, Ito H, Hayashi F, Makita T, Inada T, Tanaka M, Kimura T, Ono K. Myocardial expression level of neural cell adhesion molecule correlates with reduced left ventricular function in human cardiomyopathy. Circ Hear Fail. 2014;7:351–358.
13. Kiselyov V V., Soroka V, Berezin V, Bock E. Structural biology of NCAM homophilic binding and activation of FGFR. J Neurochem. 2005;94:1169–1179.
14. Harduin-Lepers A. The vertebrate sialylation machinery: structure-function and molecular evolution of GT-29 sialyltransferases. Glycoconj J. 2023;40:473–492.
15. Schnaar RL, Gerardy-Schahn R, Hildebrandt H. Sialic acids in the brain: Gangliosides and polysialic acid in nervous system development, stability, disease, and regeneration. Physiol Rev. 2014;94:461–518.
16. Sato C, Kitajima K. Polysialylation and disease. Mol Aspects Med. 2021;79:100892.
17. Galuska CE, Lütteke T, Galuska SP. Is polysialylated NCAM not only a regulator during brain development but also during the formation of other organs? Biology (Basel). 2017; 6:27.
18. Kudo M, Kitajima K, Inoue S, Shiokawa K, Morris HR, Dell A, Inoue Y. Characterization of the major core structures of the α2→8-linked polysialic acid-containing glycan chains present in neural cell adhesion molecule in embryonic chick brains. J Biol Chem. 1996;271:32667–32677.
19. Wuhrer M, Geyer H, Ohe M Von Der, Gerardy-Schahn R, Schachner M, Geyer R. Localization of defined carbohydrates epitopes in bovine polysialylated NCAM. Biochimie 2003; 85:207–218.
20. Park DS, Fishman GI. The cardiac conduction system. Circulation. 2011;123:904–915.
21. Doherty P, Walsh FS. CAM-FGF Receptor Interactions. Mol Cell Neurosci. 1996;8:99–111.
22. Walsh AH, Cheng A, Honkanen RE. Fostriecin, an antitumor antibiotic with inhibitory activity against serine/threonine protein phosphatases types 1 (PP1) and 2A (PP2A), is highly selective for PP2A. FEBS Lett. 1997;416:230–234.
23. Xie Y, Su N, Yang J, Tan Q, Huang S, Jin M, Ni Z, Zhang B, Zhang D, Luo F, Chen H, Sun X, Feng JQ, Qi H, Chen L. FGF/FGFR signaling in health and disease. Signal Transduct Target Ther. 2020; 5:181.
24. Carafoli F, Saffell JL, Hohenester E. Structure of the Tandem Fibronectin Type 3 Domains of Neural Cell Adhesion Molecule. J Mol Biol. 2008;377:524–534.
25. Francavilla C, Cattaneo P, Berezin V, Bock E, Ami D, Marco A De, Christofori G, Cavallaro U. The binding of NCAM to FGFR1 induces a specific cellular response mediated by receptor trafficking. J Cell Biol. 2009;187:1101–1116.
26. Everett CJ, Frithsen IL. Association of urinary cadmium and myocardial infarction. Environ Res. 2008;106:284–286.
27. Verzelloni P, Urbano T, Wise LA, Vinceti M, Filippini T. Cadmium exposure and cardiovascular

disease risk: A systematic review and dose-response meta-analysis. Environ Pollut. 2024;345:123462.

28. Lin H-C, Hao W-M, Chu P-H. Cadmium and cardiovascular disease: An overview of pathophysiology, epidemiology, therapy, and predictive value. Rev Port Cardiol. 2021;40:611–617.
29. Rasin P, V AA, Basheer SM, Haribabu J, Santibanez JF, Garrote CA, Arulraj A, Mangalaraja RV. Exposure to cadmium and its impacts on human health: A short review. J Hazard Mater Adv. 2025;17:100608.
30. Mitra S, Chakraborty AJ, Tareq AM, Emran T Bin, Nainu F, Khusro A, Idris AM, Khandaker MU, Osman H, Alhumaydhi FA, Simal-Gandara J. Impact of heavy metals on the environment and human health: Novel therapeutic insights to counter the toxicity. J King Saud Univ Sci. 2022;34:101865.
31. Slaby S, Lemière S, Hanotel J, Lescuyer A, Demuynck S, Bodart JF, Leprêtre A, Marin M. Cadmium but not lead exposure affects Xenopus laevis fertilization and embryo cleavage. Aquat Toxicol. 2016;177:1–7.
32. Slaby S, Marin M, Marchand G, Lemiere S. Exposures to chemical contaminants: What can we learn from reproduction and development endpoints in the amphibian toxicology literature? Environ Pollut. 2019;248:478–495.
33. Kolker SJ, Tajchman U, Weeks DL. Confocal imaging of early heart development in Xenopus laevis. Dev Biol. 2000;218:64–73.
34. Hoppler S, Conlon FL. Xenopus: Experimental access to cardiovascular development, regeneration discovery, and cardiovascular heart-defect modeling. Cold Spring Harb Perspect Biol. 2020;12:1–10.
35. Kaltenbrun E, Tandon P, Amin NM, Waldron L, Showell C, Conlon FL. Xenopus : An Emerging Model for Studying Congenital Heart Disease. 2011; 91:495-510.
36. Lohr JL, Yost HJ. Vertebrate model systems in the study of early heart development: Xenopus and zebrafish. Am J Med Genet - Semin Med Genet. 2000;97:248–257.
37. Marchand G, Fliniaux I, Titran P, Uchimura YT, Bodart J, Lepers AH, Cailliau K, Marin M. Cadmium induces physiological and behavioral changes associated with 180 kDa NCAM lower expression and higher polysialic acid, in the African clawed Xenopus laevis tadpoles. Ecotoxicol Environ Saf. 2024;273:116119.
38. Sedmera D, McQuinn T. Embryogenesis of the Heart Muscle. Heart Fail Clin. 2008;4:235–245.
39. Tran YTH, Saha D, del Monte-Nieto G. Cardiac trabeculation in vertebrates: Convergent evolution or evolutionary adaptations associated with heart complexity? Semin Cell Dev Biol. 2025;172:103622.

40. del Monte-Nieto G, Ramialison M, Adam AAS, Wu B, Aharonov A, Uva GD, Lauren M, Pitulescu ME, Chen H, Luis J, Pompa D, Shou W, Adams RH, Harten SK, Tzahor E, Zhou B, Richard P. NRG1 defines the building plan for trabeculation. Nature. 2018;557:439–445.

41. Watanabe M, Timm M, Fallah-Najmabadi H. Cardiac expression of polysialylated NCAM in the chicken embryo: Correlation with the ventricular conduction system. Dev Dyn. 1992;194:128–141.

42. Andersson AM, Olsen M, Zhernosekov D, Gaardsvoll H, Krog L, Linnemann D, Bock E. Age-related changes in expression of the neural cell adhesion molecule in skeletal muscle: a comparative study of newborn, adult and aged rats. Biochem J. 1993;290:641–648.

43. Probstmeier R, Bilz A, Schneider-Schaulies J. Expression of the neural cell adhesion molecule and polysialic acid during early mouse embryogenesis. J Neurosci Res. 1994;37(3):324–335.

44. Nagao K, Sowa N, Inoue K, Tokunaga M, Fukuchi K, Uchiyama K, Ito H, Hayashi F, Makita T, Inada T, Tanaka M, Kimura T, Ono K. Myocardial expression level of neural cell adhesion molecule correlates with reduced left ventricular function in human cardiomyopathy. Circ Heart Fail. 2014;7(2):351-8.

45. Gordon L, Wharton J, Moore SE, Walsh FS, Moscoso JG, Penketh R, Wallwork J, Taylor KM, Yacoub MH, Polak JM. Myocardial localization and isoforms of neural cell adhesion molecule (N-CAM) in the developing and transplanted human heart. J Clin Invest. 1990;86:1293–1300.

46. Mohun TJ, Leong LM, Weninger WJ, Sparrow DB. The morphology of heart development in Xenopus laevis. Dev Biol. 2000;218:74-88.

47. Krieg PA, Sakaguchi DS, Kintner CR. Primary structure and developmental expression of a large cytoplasmic domain form of Xenopus laevis neural cell adhesion molecule (NCAM). Nucleic Acids Res. 1989;17:10321–10335.

48. Sedmera D, Reckova M, DeAlmeida A, Sedmerova M, Biermann M, Volejnik J, Sarre A, Raddatz E, McCarthy RA, Gourdie RG, Thompson RP. Functional and morphological evidence for a ventricular conduction system in zebrafish and Xenopus hearts. Am J Physiol Heart Circ Physiol. 2003;284:H1152–1160.

49. Nagao K, Ono K, Iwanaga Y, Tamaki Y, Kojima Y, Horie T, Nishi H, Kinoshita M, Kuwabara Y, Hasegawa K, Kita T, Kimura T. Neural cell adhesion molecule is a cardioprotective factor up-regulated by metabolic stress. J Mol Cell Cardiol. 2010;48:1157–1168.

50. Nigam PK, Narain VS, Kumar A, Nigam PK. Sialic acid in cardiovascular diseases. Indian J Clin Biochem. 2006;21:54–61.

51. Decloquement M, Venuto MT, Cogez V, Steinmetz A, Schulz C, Lion C, Noel M, Rigolot V, Teppa RE, Biot C, Rebl A, Galuska SP, Harduin-Lepers A. Salmonid polysialyltransferases to generate a variety of sialic acid polymers. Sci Rep. 2023;13:1–14.

52. Venuto MT, Decloquement M, Ribera JM, Noel M, Rebl A, Cogez V, Petit D, Galuska SP, Harduin-lepers A. Vertebrate Alpha2,8-Sialyltransferases (ST8Sia): A Teleost Perspective. Int J Mol Sci. 2020;21:513.

53. Kitano M, Kizuka Y, Sobajima T, Nakano M, Nakajima K, Misaki R, Itoyama S, Harada Y, Harada A, Miyoshi E, Taniguchi N. Rab11-mediated post-Golgi transport of the sialyltransferase ST3GAL4 suggests a new mechanism for regulating glycosylation. J Biol Chem. 2021;296:100354.

54. Ferro E, Bosia C, Campa CC. RAB11-Mediated Trafficking and Human Cancers: An Updated Review. Biology 2021; 10, 26.

55. M. Xing, MC. Peterman, RL. Davis, K. Oegema, AK. Shiau SJF. GOLPH3 drives cell migration by promoting Golgi reorientation and directional trafficking to the leading edge. Mol Biol Cell. 2016;27:3828–3840.

56. Gu J, Isaji T. Specific sialylation of N-glycans and its novel regulatory mechanism. Glycoconj J. 2024;41:175–183.

57. Pothukuchi P, Agliarulo I, Russo D, Rizzo R, Russo F, Parashuraman S. Translation of genome to glycome: role of the Golgi apparatus. FEBS Lett. 2019;593:2390–2411.

58. Bard F, Chia J. Cracking the Glycome Encoder: Signaling, Trafficking, and Glycosylation. Trends Cell Biol. 2016; 26: 379–388.

59. Kellokumpu S. Golgi pH, ion and redox homeostasis: How much do they really matter? Front Cell Dev Biol. 2019;7:1–15.

60. Thévenod F. Cadmium and cellular signaling cascades: to be or not to be?. Toxicol. Appl. Pharmacol. 2009; 238: 221–239.

61. Choong G, Liu Y, Templeton DM. Interplay of calcium and cadmium in mediating cadmium toxicity. Chem. Biol. Interact. 2014; 211: 54–65

62. Mohamed KA, Kruf S, Büll C. Putting a cap on the glycome: Dissecting human sialyltransferase functions. Carbohydr Res. 2024;544:109242.

63. Potelle S, Morelle W, Dulary E, Duvet S, Vicogne D, Spriet C, Krzewinski-Recchi MA, Morsomme P, Jaeken J, Matthijs G, Bettignies G De, Foulquier F. Glycosylation abnormalities in Gdt1p/TMEM165 deficient cells result from a defect in Golgi manganese homeostasis. Hum Mol Genet. 2016;25:1489–1500.

64. Durin Z, Houdou M, Legrand D, Foulquier F. Metalloglycobiology: The power of metals in regulating glycosylation. Biochim Biophys Acta Gen Subj. 2023;1867:130412.

65. Isaji T, Im S, Gu W, Wang Y, Hang Q, Lu J, Fukuda T, Hashii N, Takakura D, Kawasaki N, Miyoshi H, Gu J. An oncogenic protein Golgi phosphoprotein 3 up-regulates cell migration via sialylation. J Biol Chem. 2014;289:20694-705.

66. Arriagada C, Cavieres VA, Luchsinger C, González AE, Muñoz VC, Cancino J, Burgos PV, Mardones GA. GOLPH3 Regulates EGFR in T98G Glioblastoma Cells by Modulating Its Glycosylation and Ubiquitylation. Int J Mol Sci. 2020;21:8880.
67. Ornitz DM, Itoh N. The fibroblast growth factor signaling pathway. Wiley Interdiscip Rev Dev Biol. 2015;4:215–266.
68. Deimling SJ, Drysdale TA. Fgf is required to regulate anterior-posterior patterning in the Xenopus lateral plate mesoderm. Mech Dev. 2011;128:327–341.
69. Simões FC, Peterkin T, Patient R. Fgf differentially controls cross-antagonism between cardiac and haemangioblast regulators. Development. 2011;138:3235–3245.
70. Rochais F, Mesbah K, Kelly RG. Signaling pathways controlling second heart field development. Circ Res. 2009;104:933–942.
71. Kloesel B, Dinardo JA, Body SC. Cardiac Embryology and Molecular Mechanisms of Congenital Heart Disease: A Primer for Anesthesiologists. Anesth Analg. 2016;123:551-569.
72. Dell'Era P, Ronca R, Coco L, Nicoli S, Metra M, Presta M. Fibroblast growth factor receptor-1 is essential for in vitro cardiomyocyte development. Circ Res. 2003;93:414–420.
73. Khosravi F, Ahmadvand N, Bellusci S, Sauer H. The Multifunctional Contribution of FGF Signaling to Cardiac Development, Homeostasis, Disease and Repair. Front Cell Dev Biol. 2021;9:1–22.
74. Itoh N, Ohta H, Nakayama Y, Konishi M. Roles of FGF signals in heart development, health, and disease. Front Cell Dev Biol. 2016;4:1–11.
75. Itoh N, Ohta H. Pathophysiological roles of FGF signaling in the heart. Front Physiol. 2013;4:2–5.
76. Chen X, Qian J, Liang S, Qian J, Luo W, Shi Y, Zhu H, Hu X, Wu G, Li X, Liang G. Hyperglycemia activates FGFR1 via TLR4/c-Src pathway to induce inflammatory cardiomyopathy in diabetes. Acta Pharm Sin B. 2024;14:1693–1710.
77. Marguerie A, Bajolle F, Zaffran S, Brown NA, Dickson C, Buckingham ME, Kelly RG. Congenital heart defects in Fgfr2-IIIb and Fgf10 mutant mice. Cardiovasc Res. 2006;71:50–60.
78. Chia J, Goh G, Racine V, Ng S, Kumar P, Bard F. RNAi screening reveals a large signaling network controlling the Golgi apparatus in human cells. Mol Syst Biol. 2012;8:629.
79. Zamai M, Trullo A, Giordano M, Corti V, Cuesta EA, Francavilla C, Cavallaro U, Caiolfa VR. Number and brightness analysis reveals that NCAM and FGF2 elicit different assembly and dynamics of FGFR1 in live cells. J Cell Sci. 2019;132:jcs1–10.
80. Fan GP, Wang W, Zhao H, Cai L, Zhang P De, Yang ZH, Zhang J, Wang X. Pharmacological Inhibition of Focal Adhesion Kinase Attenuates Cardiac Fibrosis in Mice Cardiac Fibroblast and Post-Myocardial-Infarction Models. Cell Physiol Biochem. 2015;37:515–526.
81. Gilbert CJ, Longenecker JZ, Accornero F. ERK1/2: An Integrator of Signals That Alters Cardiac

Homeostasis and Growth. Biology (Basel). 2021;10:1–19.

82. Niethammer P, Delling M, Sytnyk V, Dityatev A, Fukami K, Schachner M. Cosignaling of NCAM via lipid rafts and the FGF receptor is required for neuritogenesis. J Cell Biol. 2002;157:521–532.
83. Xu Z, Isaji T, Fukuda T, Wang Y, Gu J. O-GlcNAcylation regulates integrin-mediated cell adhesion and migration via formation of focal adhesion complexes. J Biol Chem. 2019;294:3117–3124.
84. Zhang Z, Isaji T, Oyama Y, Liu J, Xu Z, Sun Y, Fukuda T, Lu H, Gu J. O-GlcNAcylation of Focal Adhesion Kinase Regulates Cell Adhesion, Migration, and Proliferation via the FAK/AKT Pathway. Biomolecules. 2024;14:1577.
85. Wu M. Mechanisms of Trabecular Formation and Specification During Cardiogenesis. Pediatr Cardiol. 2018;39:1082-1089.
86. Nakamura T, Colbert M, Krenz M, Molkentin JD, Hahn HS, Dorn GW, Robbins J. Mediating ERK1/2 signaling rescues congenital heart defects in a mouse model of Noonan syndrome. J Clin Invest. 2007;117:2123–2132.
87. Rivero-García P, Campuzano-Estrada I del C, Hernandez-Felix JH. Hypertrophic cardiomyopathy in an adult patient with Noonan syndrome with multiple lentigines. Clin Case Reports. 2023;11:e7607.
88. Marino B, Digilio MC, Toscano A, Giannotti A, Dallapiccola B. Congenital heart diseases in children with Noonan syndrome: An expanded cardiac spectrum with high prevalence of atrioventricular canal. J Pediatr. 1999;135:703–706.
89. Rocca Serra-Nédélec A De, Edouard T, Tréguer K, Tajan M, Araki T, Dance M, Mus M, Montagner A, Tauber M, Salles JP, Valet P, Neel BG, Raynal P, Yart A. Noonan syndrome-causing SHP2 mutants inhibit insulinlike growth factor 1 release via growth hormone-induced ERK hyperactivation, which contributes to short stature. Proc Natl Acad Sci U S A. 2012;109:4257–4262.
90. Linglart L, Gelb BD. Congenital heart defects in Noonan syndrome : Diagnosis, management, and treatment. Am J Med Genet C Semin Med Genet. 2020;184:73-80.
91. Stachowiak MK, Stachowiak EK. Evidence-Based Theory for Integrated Genome Regulation of Ontogeny-An Unprecedented Role of Nuclear FGFR1 Signaling. J Cell Physiol. 2016;231:1199–1218.
92. Dunham-Ems SM, Lee YW, Stachowiak EK, Pudavar H, Claus P, Prasad PN, Stachowiak MK. Fibroblast Growth Factor Receptor-1 (FGFR1) Nuclear Dynamics Reveal a Novel Mechanism in Transcription Control. Mol Biol Cell. 2009;20:2401–2412.
93. Warkman AS, Krieg PA. Xenopus as a model system for vertebrate heart development. Semin Cell Dev Biol. 2007;18(1):46-53.
94. Nieuwkoop, P, Faber, J. A Systematical and Chronological Survey of the Development from the

Fertilized Egg till the End of Metamorphosis, Edited by J. Faber, P. D. Nieuwkoop, Garland Publishing Inc, 1994, New York ISBN 0-8153-1896-0.

95. Cailliau K, Marcis V Le, Béréziat V, Perdereau D, Cariou B, Vilain JP, Burnol A-F, Browaeys-Poly E. Inhibition of FGF receptor signaling in Xenopus oocytes: Differential effect of Grb7, Grb10 and Grb14. FEBS Lett 2003;548:43–48.

Figure legends

Fig. 1: Experimental design. Experiments were conducted either (**A**) on isolated *Xenopus* hearts in figures 2, 3, 4, and 5 or (**B**) on *Xenopus* oocytes expressing the FGFR1 receptor in figure 6, as described in the Material and Method section. n indicates the number of sialic acid residues present in the PSA chain on heart NCAM.

Fig. 2: Cadmium blocks ventricle trabeculae formation. (**A**) Histological analysis of *Xenopus* hearts was performed on control (**a, b, c**) and 15 µM cadmium-treated samples (**d, e, f**) at stage 45, using transversal serial sections stained with nuclear red and picroindigo carmine. By stage 45 in (**a, b, c**), a heart with three chambers has developed. Paired aortic arch arteries (AA) connect at the outflow tract (OFT), which contains a spiral septum (SS) and leads to a single ventricle (V) with thin trabeculated myocardium (see arrows in b and c). The left and right atria (Al, Ar) lie dorsal to the ventricle and are separated by an atrial septum (As). Some blood is trapped inside the heart chambers. Following cadmium treatment, the heart exhibits a reduced ventricle with a thick myocardium lacking trabeculae (asterisk in **e** and **f**). (**B**) Statistical analyses were conducted on n=18 tadpoles from N=2 independent fertilizations. The data are presented as the mean ± SD, and statistical analysis revealed a significant difference in the number of trabeculae (Mann-Whitney, ** $p < 0.01$). Scale bar=100 µm.

Fig. 3: Cadmium exposure increases PSA on NCAM but not NCAM in tadpoles' heart. Western blot analyses were conducted using antibodies targeting PSA, NCAM, or Actin on (**A**) whole cell extracts and (**B**) immunoprecipitated NCAM obtained from control samples (C) or tadpoles exposed to 15 µM cadmium until stage 45 (Cd). In (**A**)**,** lanes 3 and 4, the extracts were treated with endoneuraminidase (EndoN) before electrophoresis and western Blot. In (**B**)**,** immunoprecipitations were performed with either IgG (lanes 1 and 2) or NCAM (lanes 3, 4, 5 and 6). Lanes 5 and 6 represent the lysate samples remaining after NCAM immunoprecipitations. Statistical analyses were carried out on 20 pooled hearts and on N=5 independent fertilizations. The data are presented as the mean ± SD. In (**A**), statistical

analysis showed significantly more PSA in Cd-treated hearts than in controls (Student's t test, ***p < 0.001). In (**B**), statistical analysis showed significantly more PSA on NCAM in Cd-treated hearts (Mann-Whitney, **p < 0.01).

Fig. 4: *NCAM*, sialidase *Neu1, and* polysialyltransferases *ST8sia2* and *ST8sia4* mRNA are not increased under cadmium exposure. Absolute number of *NCAM*, *sialidase Neu1, ST8sia2,* and *ST8sia4* transcripts in hearts of control and cadmium-treated (Cd-treated) stage 45 *Xenopus* was assessed by RT-qPCR and normalized with *histone H4*. (**A**) Average mRNA copy number per 10^4 copies of *histone H4* in hearts of control and cadmium-treated tadpoles. No statistical difference was revealed between the two groups. (**B**) Relative mRNA expression of cadmium-treated hearts *versus* control within each independent fertilization. Hearts from 50 *Xenopus* at stage 45 are pooled, and N=6 independent fertilizations are performed. Data are presented as mean ± SD.

Fig. 5: Changes in molecular effectors in stage 45 tadpole hearts and their Golgi apparatus after cadmium exposure. Western blots were performed on hearts from untreated (C) and 15 µM cadmium-treated tadpoles (Cd) after preparation of whole extracts (**A, B**), FGFR1-, Integrin-, and FAK-immunoprecipitations (**C, D, E**), WGA column (**F**), or purified Golgi apparatus (**G**). Antibodies against FGFR1, phosphorylated tyrosine (PY), PSA-NCAM, Src, Shp2, Integrin, FAK, Golph3, Rab11, Erk2, phosphorylated Erk2 (P-Erk2), *O*-GlcNAcylation, GM130, TGN46, and Actin were used on the same blot, followed by membrane reblotting. Statistical analyses were realized on groups of 20 pooled hearts at stage 45 and on N=4 independent fertilizations, except for NCAM in Figure 5A, where N=5. Data are shown as mean ± SD; statistical significance was assessed with Student's t-test: *p < 0.05, **p < 0.01, ***p < 0.001.

Fig. 6: Reconstitution of the PSA-NCAM/FGFR signaling confirms cadmium-induced rewiring. Western blots were performed directly after immunoprecipitation with IgG or NCAM antibodies and followed by an elution of control NCAM (NCAM) and cadmium-treated NCAM (NCAMCd) with or without endoneuraminidase (EndoN) treatment from tadpole hearts at stage 45 (**A**). FGFR1 was expressed in the model system of *Xenopus* oocytes and stimulated by FGF2, eluted control NCAM, or eluted NCAMCd before immunoprecipitations with antibodies against respectively FGFR1 (**B** and **F**), Integrin (**C**), FAK (**D** and **G**), direct western blot (**E**), or from separated membrane, cytosol, and nuclear fractions (**H**). In **F, G, H**, lanes 5, 6, and 7, an antibody raised against FAK was microinjected into the FGFR1 expressing system 1 h before stimulation by ligands FGF2, eluted control NCAM, or eluted NCAMCd. Western blots were performed against FGFR1, phosphorylated tyrosine (PY), Grb2, Src, Shp2, Integrin, FAK, Golph3, Rab11, Erk2, phosphorylated Erk2 (P-Erk2), *O*-GlcNAcylation, and Actin

after stripping and reblotting membranes. Statistical analyses were carried out in groups of 10 pooled expressing oocytes and on N=4 independent fertilizations. Data are shown as mean ± SD; statistical significance was assessed with Student's t-test: ***$p < 0.001$.

Fig. 7: Signaling modifications in the developing heart after cadmium exposure. Heart features in control (**A**) change under cadmium exposure (**B**), resulting in no ventricular myocardial trabeculae, altered Golgi apparatus enzymes, and disrupted PSA-NCAM/FGFR signaling. Normally, in controls, the Golgi contains Rab11, Golph3, and polysialyltransferases. Additionally, PSA-NCAM complexes with FGF receptor and Integrin, recruiting FAK, low Shp2, and allowing Erk2 phosphorylation and nuclear translocation of FGFR. Cadmium deregulation increases PSA on NCAM, and favors a decrease of Rab11, a rise in Golph3, and an accumulation of sialyltransferases ST8Sia2 and ST8Sia4 in the Golgi apparatus. The excess of PSA on NCAM rewires FGFR signaling, bypassing Integrin/FAK and allowing FAK *O*-GlcNAcylation. The PSA-NCAM/FGFR signaling further recruits a higher amount of Shp2, resulting in an increase in Erk2 phosphorylation and a defect in FGFR nuclear addressing. The latest features are some of the hallmarks of heart pathologies and congenital diseases. Interactions are indicated by arrows.

Supplementary figure

Mean ± standard deviation values (SD) for data presented in the histograms of figures 2, 3, 4, 5, and 6.

Figure 1

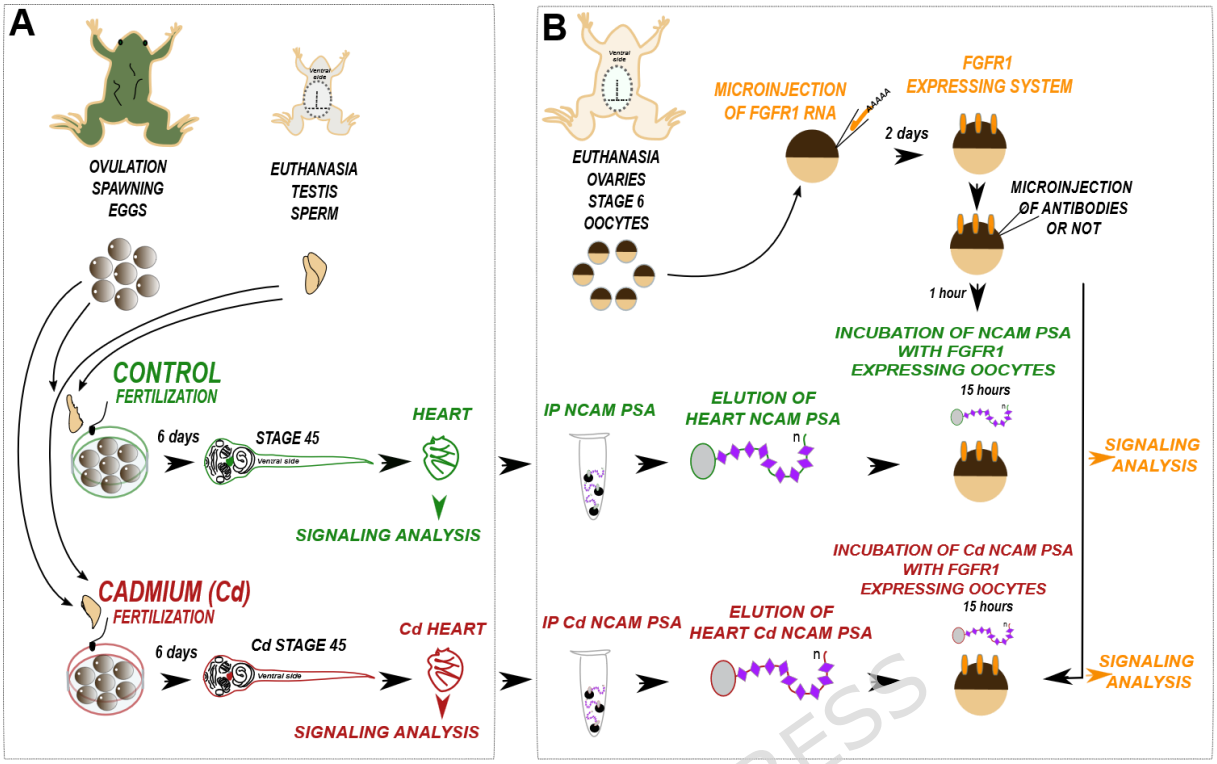

Figure 2

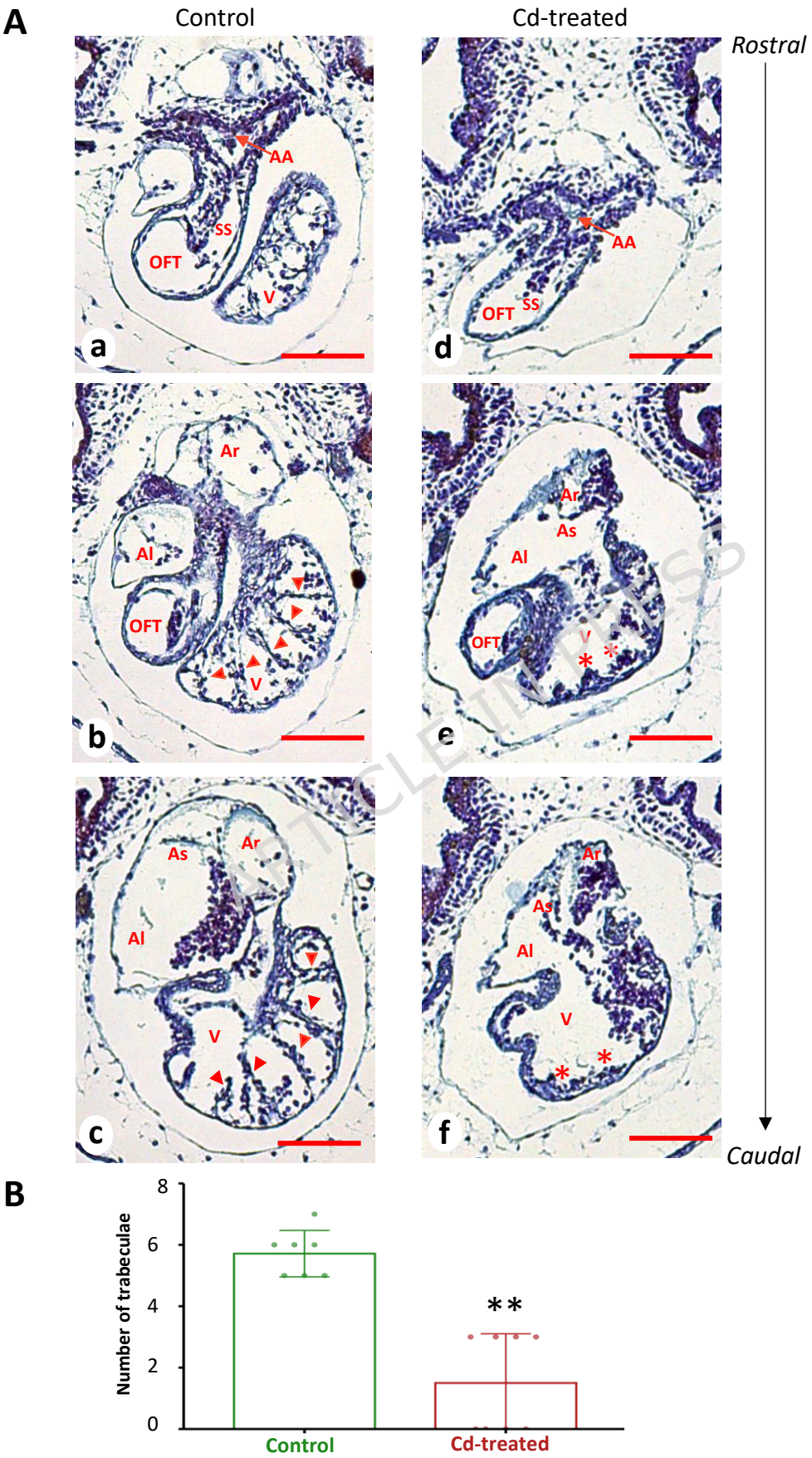
A
Control
Cd-treated
Rostral
Caudal
AA
SS
OFT
V
a
d
Ar
Al
b
As
e
c
f
B
Number of trabeculae
8
6
4
2
0
**
Control
Cd-treated

Figure 3

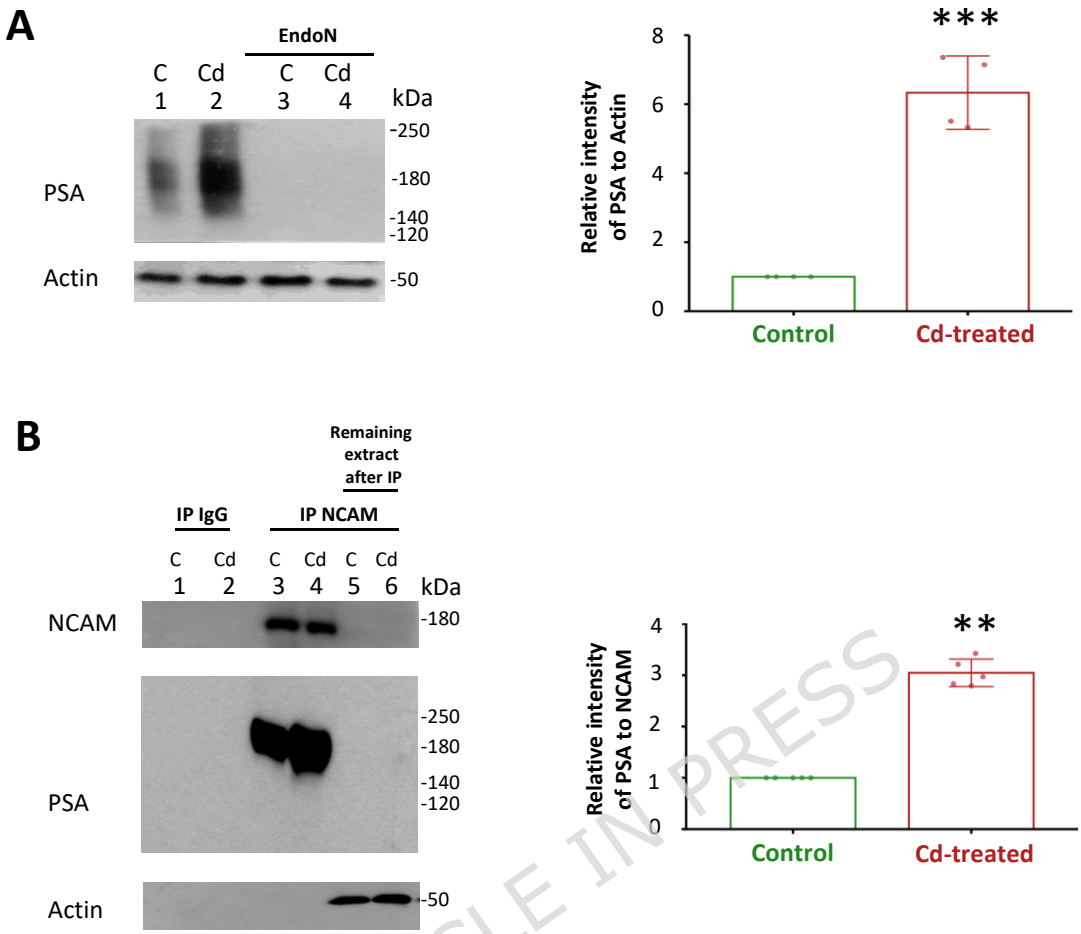

Figure 4

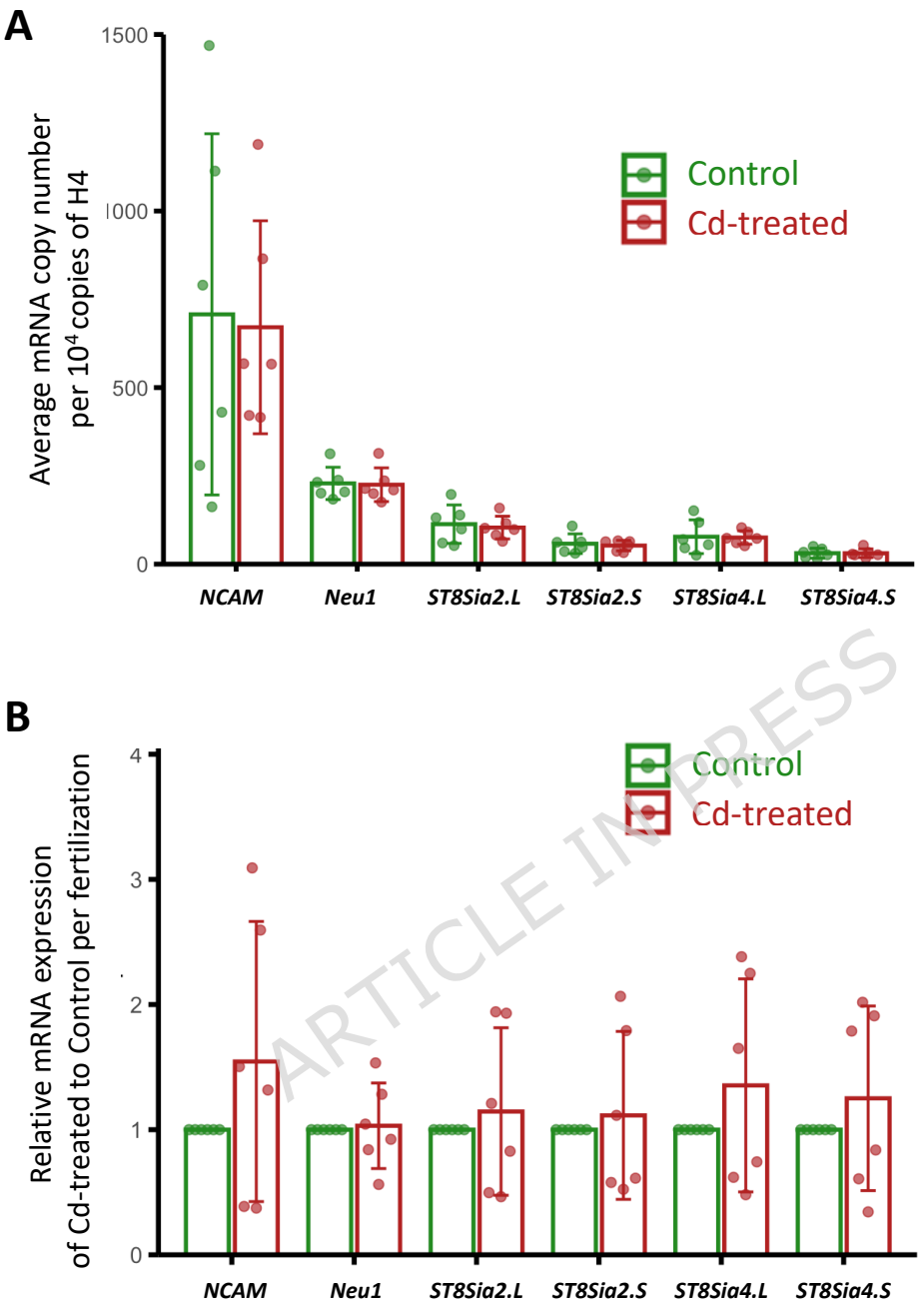

Figure 5

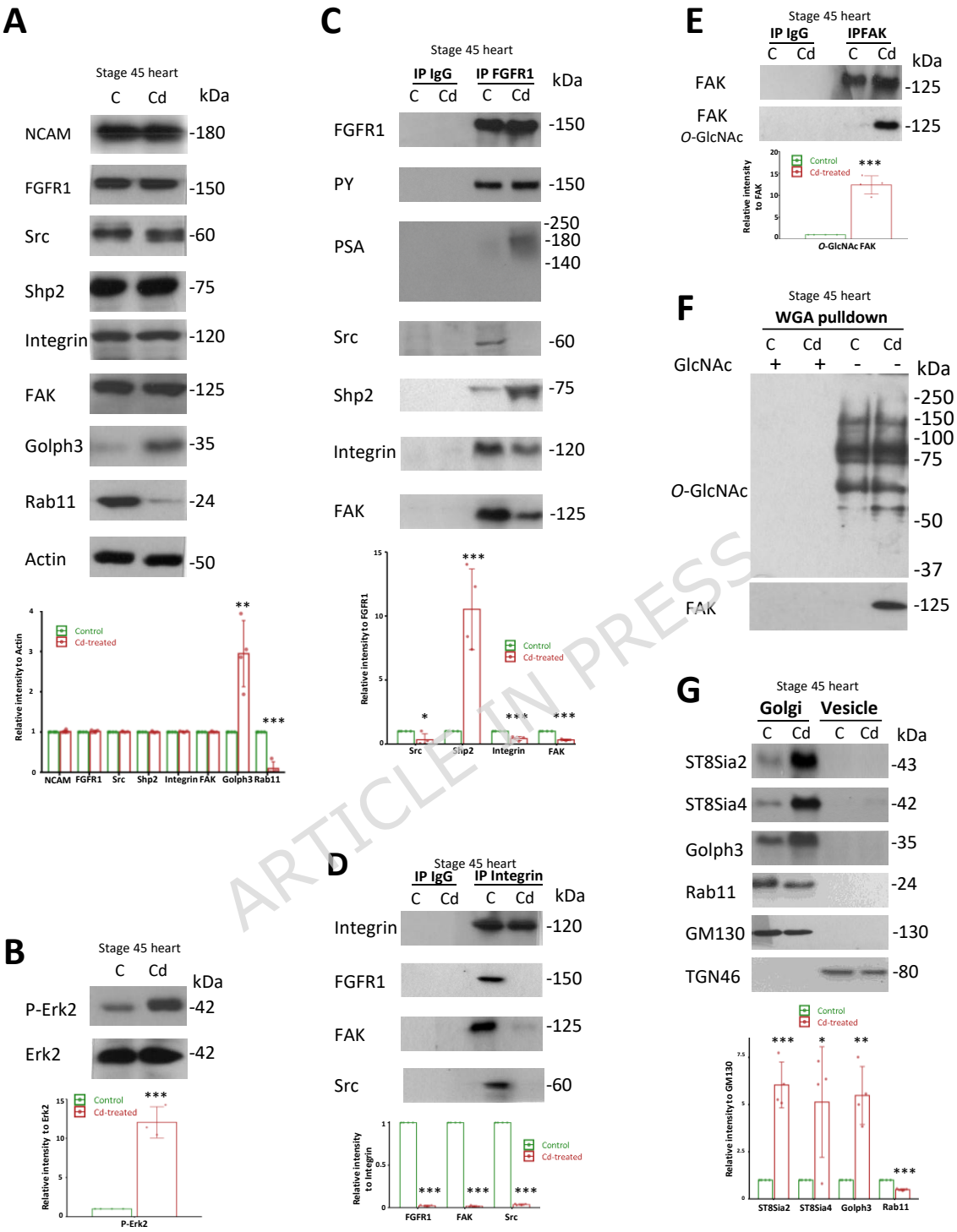

Figure 6

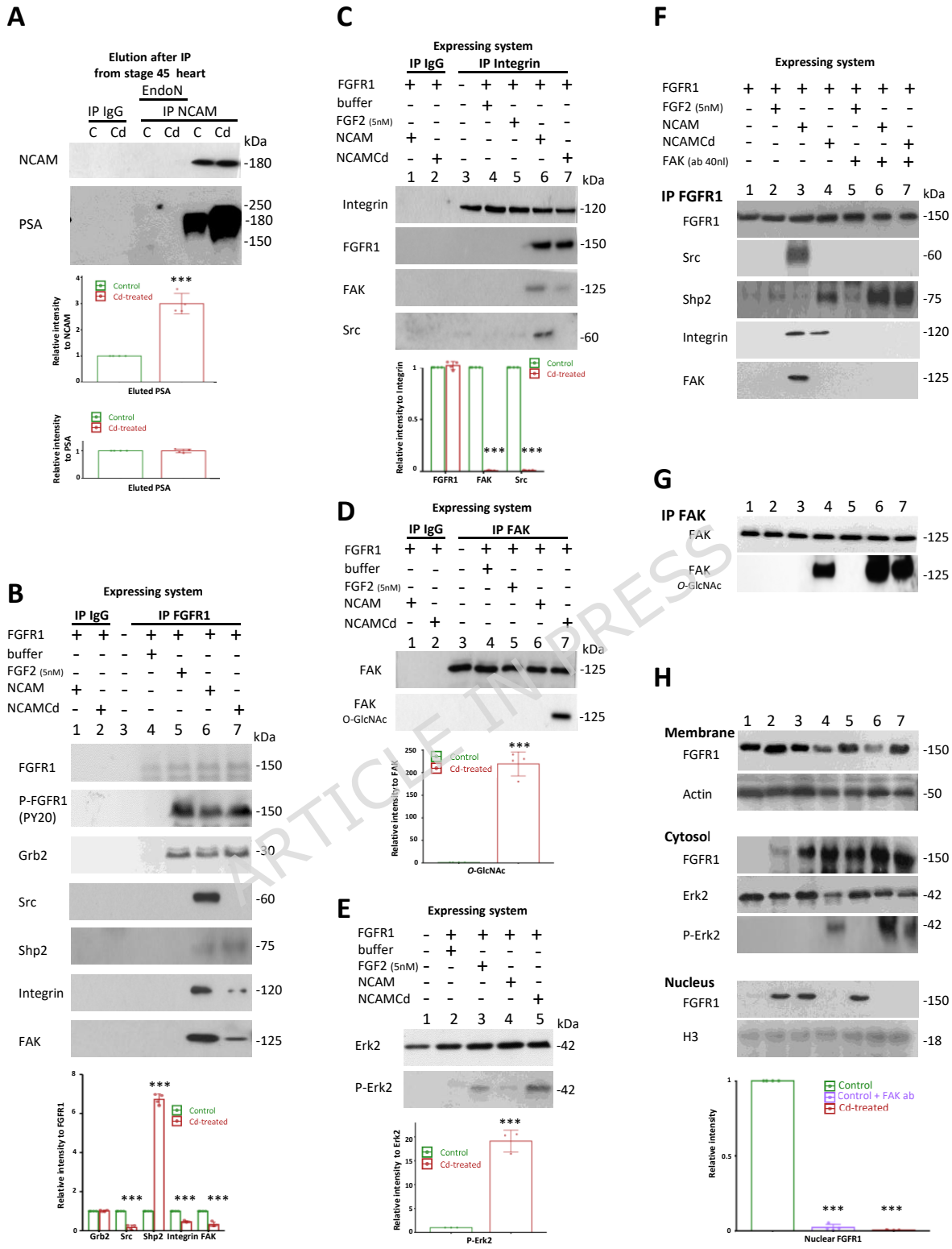

Figure 7